Consistent with the reported results in SIV239-infected animals, no appreciable nAb titre was detected in two animals (Mm13 and Mm25), despite the fact that viral load in Mm13 was distinctively decreased by 30 weeks p.i. However, we observed a rare animal (Mm20) that elicited a robust nAb response against SIV239 and a relatively delayed nAb response against Δ5G, despite the maintenance of a high viral load (Fig. 2a). These results indicated the lack of correlation of nAb response with viral load in SIV239-infected animals. In contrast, nAb was detected in two Δ5G-infected animals (Mm07 and Mm22) starting at 8 weeks p.i. and in two additional animals (Mm12 and Mm23) at 12 weeks p.i. (Fig. 2b, left panel). These titres peaked at either 12 or 18 weeks p.i., and the peak was followed by a decrease in titre that varied among animals. Mm12 and Mm23, which exhibited nAb induction at 12 weeks p.i., had essentially low titres, whilst Mm07 and Mm22, which exhibited nAb induction at an earlier time point, maintained vigorous nAb titres of >1 : 100. Of note, plasma from Mm26 did not contain detectable levels of nAb at any time p.i. In contrast, nAb against SIV239 was not induced in any of the Δ5G-infected animals (Fig. 2b, right panel). As low-level nAb may play a role in control of virus replication, purified IgG from the plasma samples was used to measure neutralizing activity. However, the results from the purified IgG corresponding to the plasma at a 1 : 3 dilution did not change the kinetics of nAb response in Δ5G-infected animals (data not shown).

In experiments where the passive administration of monoclonal HIV nAb successfully prevented the infection of macaques with simian–human immunodeficiency virus, the results unequivocally indicated that high titres of nAb were needed to achieve such protection (Nishimura *et al.*, 2002). In consideration of these results, data were recalculated based on a cut-off value of 90 % inhibition of virus replication (IC_{90}) in $CD4^+$ T-cell lines. As a result, nAb responses were detected in only two of the animals, Mm07 and Mm22, but with titres of 1 : 100 and 1 : 500, respectively (Fig. 2b, middle panel). Next, we examined the correlation between viral load and nAb titre at 8 and 12 weeks p.i. and found that the correlation was not statistically significant (Fig. 2c).

Anti-gp120 Ab response in Δ5G-infected animals

Next, we measured binding Ab responses against gp120. When the plasma samples were assayed for levels of Ab that bound to SIV239 gp120 or Δ5G gp120, essentially identical values were obtained. Fig. 3 shows the data obtained using SIV239 gp120. Remarkably, anti-gp120 responses during the early period p.i. between the two groups of monkeys were distinct. Whereas anti-gp120-specific Ab responses

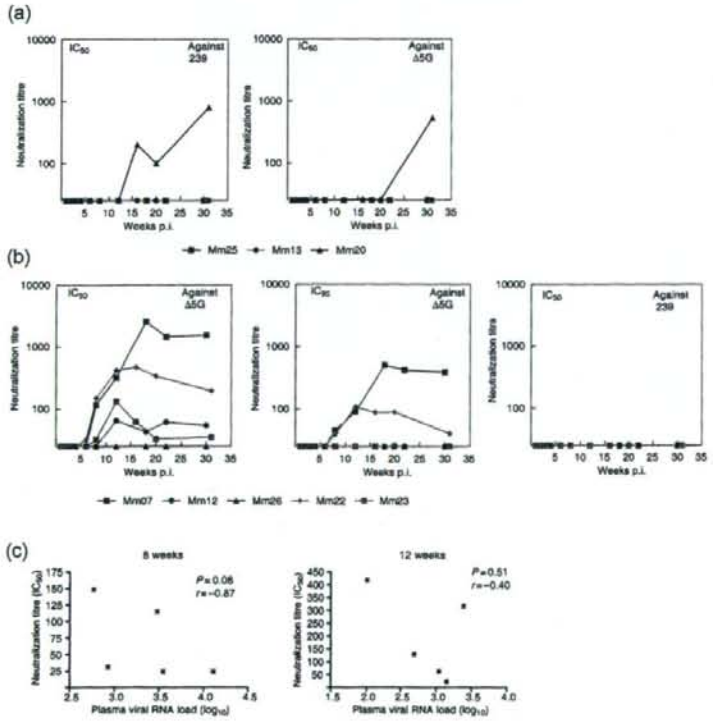

Fig. 2. nAb titres in SIV-infected animals. (a) nAb titres in SIV239-infected animals are indicated as the plasma dilution yielding 50 % inhibition (IC_{50}) of SIV239 infection (left) or Δ5G infection (right) in CEMx174/SIVLTR-SEAP cells. (b) nAb titres in Δ5G-infected animals are indicated as the plasma dilution that yielded 50 % inhibition (IC_{50}, left) and 90 % inhibition (IC_{90}, middle) of Δ5G infection or 50 % inhibition of SIV239 infection (right) in CEMx174/SIVLTR-SEAP cells. (c) Correlation between IC_{50} nAb titres and plasma viral RNA load at 8 and 12 weeks p.i. in Δ5G-infected animals.

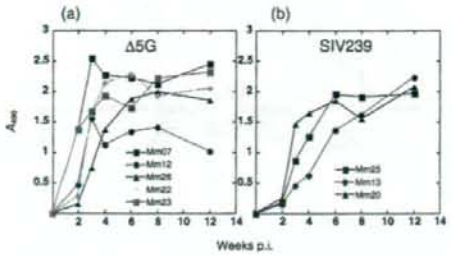

Fig. 3. Anti-gp120 Ab responses. Anti-gp120 Ab responses in Δ5G-infected (a) and SIV239-infected (b) animals were indicated as A_{490} using plasma diluted 1 : 100 in an ELISA.

peaked at 3–4 weeks p.i. in Δ5G-infected animals (Fig. 3a), those in SIV239-infected animals remained generally lower and required longer periods of time to reach their peak (Fig. 3b). Of note, whilst anti-gp120 Ab responses did not correlate well with nAb titres in the chronic phase in Δ5G-infected animals, the hierarchy detected in nAb titres (Mm07, Mm22, Mm23, Mm12 and Mm26, in descending order) was similar to that observed for gp120-binding antibodies at 2 weeks p.i. (Fig. 3a).

Ab responses to linear epitopes in gp120 and gp41 in Δ5G-infected animals differ from those detected in SIV239-infected animals

Next, we examined Ab-binding responses to linear epitopes in plasma samples from infected animals at 8 weeks p.i., as both nAb and anti-gp120-binding Ab were detected at this time point (Figs 2 and 3). We used 72 overlapping peptides encompassing the entire Env sequence of SIV239 for the detection of epitope-specific Ab in plasma samples from Δ5G-infected or SIV239-infected animals. As shown in Fig. 4 and Table 1, the plasma samples reacted with the peptides in six regions: two in gp120 and four in gp41. The regions in gp120 resided in the vicinity of V1/V2, designated region 1 (aa 109–193), and at the C terminus, designated region 2 (aa 493–529). Of note, only linear region 1 was directly affected by selected deglycosylation (aa 146 and 171). The regions in gp41 were located in the ectodomain for region 3 (aa 589–625) and region 4 (aa 660–685), and in the cytoplasmic domain for region 5 (aa 721–757) and region 6 (aa 841–879).

Although Ab responses to most of the peptides recognized in the plasma samples from Δ5G-infected animals were similar to those in SIV239-infected animals, a few peptides were recognized by Abs only in samples from Δ5G-infected animals, and Ab reactivity to some peptides was significantly different between the two groups (Fig. 4b, c and Table 1). Firstly, in region 1, whereas five peptides (Env-10, -12, -13, -14 and -15) were recognized by Abs from Δ5G-infected animals, only three peptides (Env-10, -12 and -13) reacted with Abs from SIV239-infected animals (Fig. 4b and c). Peptide Env-10 was detected by Abs from four Δ5G-infected animals, but from only one of the SIV239-infected animals. Similarly, peptides Env-12 and -13 were detected by Abs from five Δ5G-infected animals and two SIV239-infected animals. In contrast, peptides Env-14 and -15 were detected by Abs from Δ5G-infected animals but not SIV239-infected animals. The specificity of Δ5G infection in the reactivity of peptide Env-14 was statistically significant (P=0.0149) (Table 1). Secondly, the reactivity of Ab from Δ5G-infected animals with the peptides in regions 2, 3 and 4 was lower than that recorded with Ab from SIV239-infected animals (Fig. 4b and c). As shown in Table 1, the reduction in Ab reactivity from Δ5G-infected animals to peptide Env-51 (region 3) and peptide Env-56 (region 4) was significant (P=0.014 and 0.0053, respectively); however, the reduction in Ab response in region 2 was not significant. In addition, there were no significant differences in the Ab responses to the peptides in regions 5 and 6 between Δ5G-infected and SIV239-infected monkeys (Fig. 4b, c and Table 1).

A Δ5G-specific linear epitope resides in the region containing the third deglycosylation site (aa 171) between V1 and V2

As region 1 also contained the site of two mutations introduced to limit glycosylation in the Δ5G mutant, we focused additional studies on this region. To identify the Δ5G-specific epitope(s) in region 1, peptide ELISA was performed with 12 newly synthesized shorter peptides based on the Δ5G sequence spanning the V1/V2 region (Fig. 5). Ab reactivity to peptide Env-14 was mapped to peptides V1V2-9–11 (Fig. 5a). Thus, three linear epitopes (encompassed in peptides Env-10, V1V2-3 and V1V2-9–11) were identified within the V1/V2 region (Figs 4 and 5). Whilst two epitopes contained in peptides Env-10 and V1V2-3 were recognized by Ab from both SIV239- and Δ5G-infected animals, the epitope(s) corresponding to peptides V1V2-9–11 was specific to Δ5G infection (Fig. 5a). As the latter contained the third deglycosylation mutation (Figs 1 and 5b, aa 171), Δ5G specificity was probably secondary to the removal of *N*-glycan at this site in SIV239 gp120 (Fig. 5).

Δ5G-specific Ab responses to linear epitopes in Env elicited immediately following primary infection

In an effort to define the potential relevance of the linear epitope-specific Ab responses in the reduction of acute virus replication in Δ5G-infected animals, we examined the kinetics of Ab reactivity to 12 peptides: Env-10, V1V2-3 and V1V2-9, -10 and -11 for epitopes in region 1; Env-42 and -43 for epitopes in region 2; Env-50 and -51 for epitopes in region 3; Env-56 for epitopes in region 4; and Env-61 and -62 for epitopes in region 5 (Fig. 6). Whilst the induction kinetics of Ab to most peptides were variable in

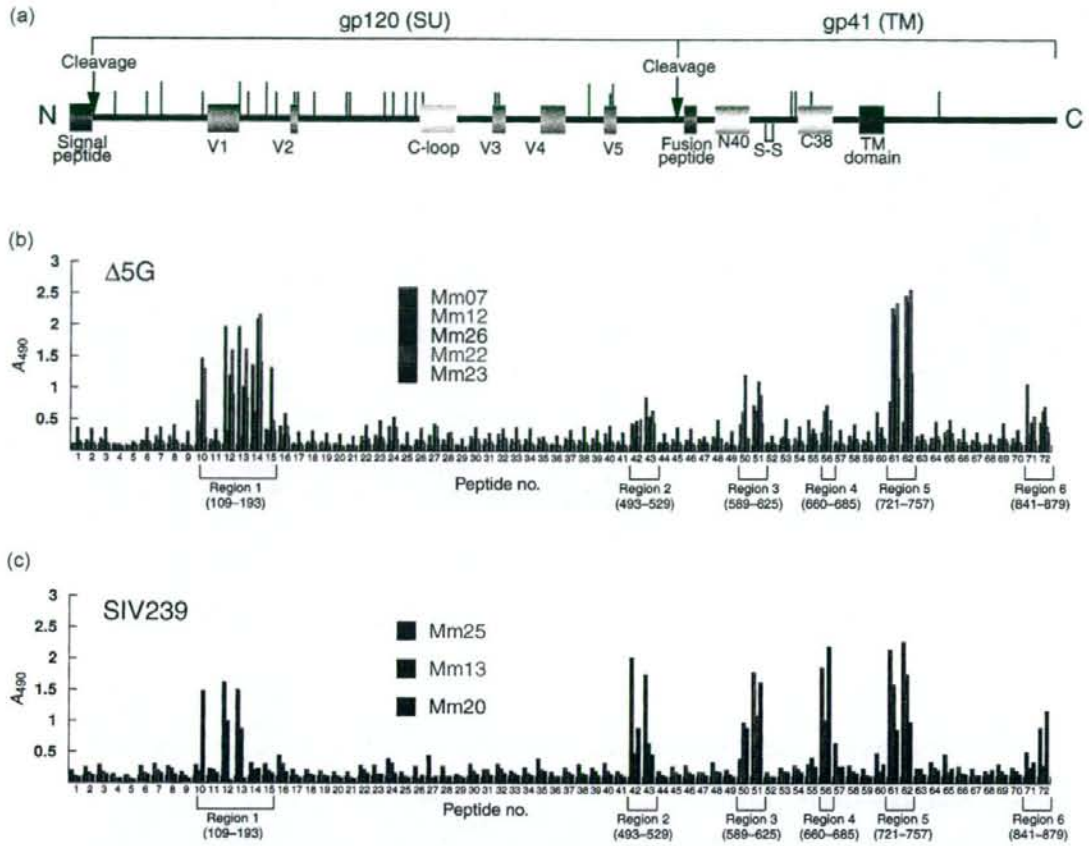

Fig. 4. Ab reactivity to synthetic overlapping peptides spanning the entire Env protein. (a) Diagram of SIV239 Env with the locations of the signal peptide (violet box), variable regions (pink boxes), cysteine loop (yellow box), fusion peptide (green box), N-terminal (N40) and C-terminal (C38) heptad repeats (light-blue boxes), membrane-spanning domain (blue box) and *N*-glycosylation sites (vertical bars) (Burns & Desrosiers, 1991; Choi *et al.*, 1994; Liu *et al.*, 2002). Red vertical bars indicate deglycosylation sites (aa 79, 146, 171, 460 and 479) in Δ5G. S-S indicates the indispensable disulfide bond for hairpin loop formation of the TM protein. (b, c) Plasma samples collected from animals infected with Δ5G (b) and SIV239 (c) at 8 weeks p.i. were used to examine Ab reactivity to 72 peptides (25 mers) overlapping by 13 residues each and spanning the entire Env protein. Reactivity was shown by A_{490}.

plasma from both groups of animals, Ab to V1V2-9, -10 and -11 was specific for Δ5G-infected animals, with rapid induction following primary infection. Ab responses to Env-61 and -62 were also induced rapidly in animals from the two groups; however, it has already been confirmed by SIV and HIV studies that a linear epitope covered by these peptides is the immunodominant epitope with no association with virus control (Eberle *et al.*, 1997; Kent *et al.*, 1992). In contrast to Ab responses to V1/V2 peptides, whilst Ab to peptides Env-51 and -56 in the gp41 ectodomain were detected in SIV239-infected animals, these reactions were low until at least 12 weeks p.i. in Δ5G-infected animals.

Properties of Ab against Δ5G-specific linear epitope

Although Ab reactivity to peptide V1V2-9, -10 and -11 was elicited specifically in Δ5G-infected animals, these Abs were non-nAbs, as these binding Abs were detected in all Δ5G-infected animals, including a nAb-undetectable monkey (Mm26), and before nAb was detected. In addition, we attempted to inhibit neutralization by the addition of excess concentrations of V1V2-9, -10 and -11 to the neutralization assay performed with plasma from Δ5G-infected animals collected at 8 and 12 weeks p.i. The reduction of nAb by the addition of an excess amount of

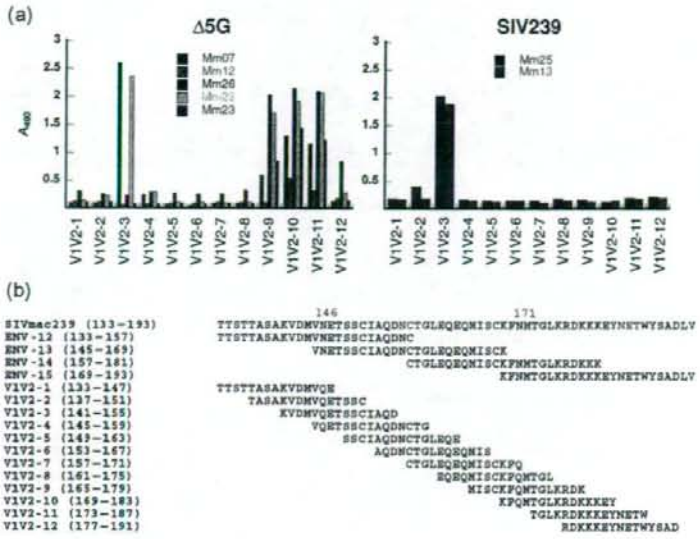

Fig. 5. Ab reactivity to linear epitopes in the V1/V2 region of gp120. (a) To define linear epitopes in the V1/V2 region, peptide ELISA was performed using 12 peptides (15 mers) overlapping by 11 residues each. (b) Sequences and positions of the 12 V1/V2 peptides used in (a) and the peptides Env-12 to -15.

peptide was not detected in any samples, confirming that the epitopes targeted by nAb and V1V2-specific Ab were distinct (data not shown).

Next, we tested plasma IgG samples from SIV-infected animals for the quantitative capture of whole virions. IgG fractions of plasma samples from SIV-infected animals collected at 3–4 weeks p.i. were compared for their capacity to capture Δ5G or SIV239 virions. IgG fractions from two Δ5G-infected animals (Mm07 and Mm22) exhibited remarkably higher virion capture activity than those from other animals (Fig. 7a); however, this capture activity was

Table 1. Epitope-specific Ab-binding regions in Env and influence of deglycosylation on Ab binding

Env subunit	Ab-binding region	Peptide no.	Amino acid range	Region	*P* value*
SU	Region 1	10	109–133	V1	0.6733
		12	133–157	V1	0.5678
		13	145–169	V1/V2	0.5563
		14	157–181	V1/V2	0.0149†
		15	169–193	V1/V2	0.2385
	Region 2	42	493–517	SU C terminus	0.0822
		43	505–529		0.3039
TM	Region 3	50	589–613	Ectodomain	0.4791
		51	601–625		0.0140†
	Region 4	56	660–685	Ectodomain	0.0053‡
	Region 5	61	721–746	Cytoplasmic domain	0.6818
		62	732–757		0.8188
	Region 6	71	841–865	Cytoplasmic domain	0.5237
		72	853–879		0.2451

*A *t*-test was performed by using data in Fig. 4 to determine differences in Ab reactivity between SIV239 infection and Δ5G infection.
†$P<0.05$; ‡$P<0.01$.

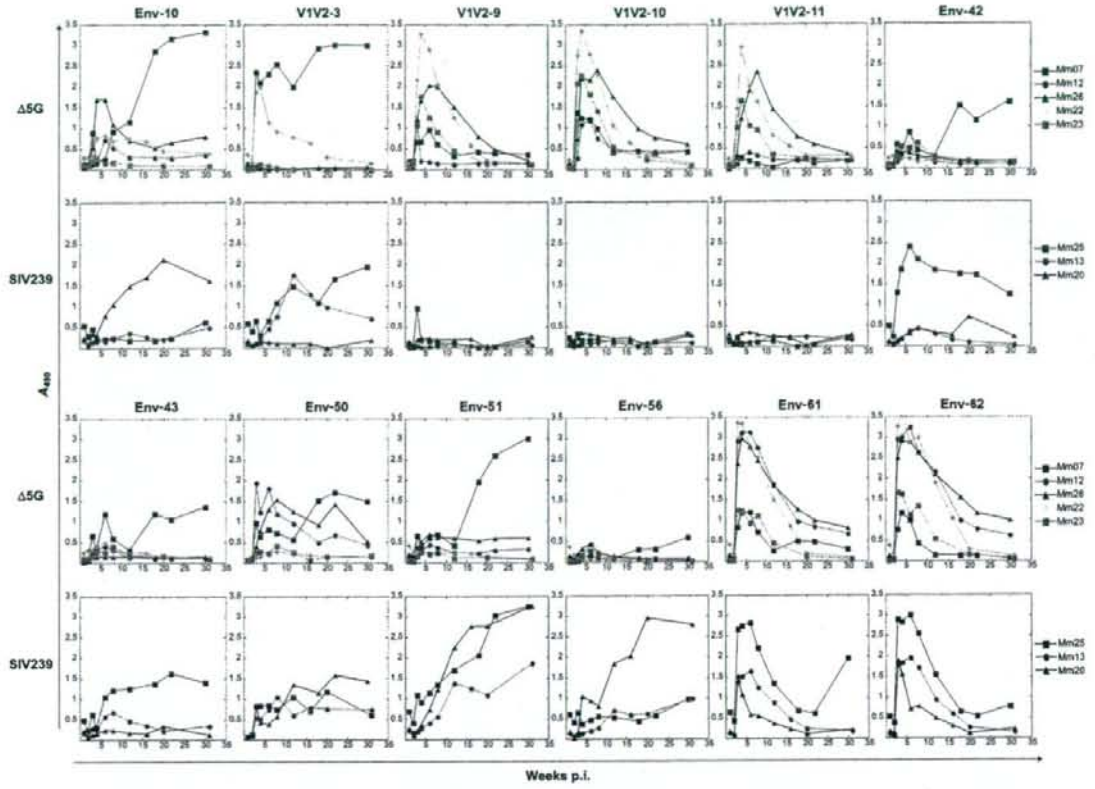

Fig. 6. Kinetics of peptide-specific Ab responses in Δ5G-infected and SIV239-infected animals. The kinetics of Ab reaction against peptides selected in the experiments shown in Figs 4 and 5 was determined as A_{490} using plasma diluted 1 : 100 in an ELISA.

Δ5G-specific, as no appreciable capture of SIV239 virion was detected with these samples. Furthermore, this activity was reduced to the level of control IgG (R374) after selective removal of IgG binding to V1V2-9, -10 and -11 peptides, suggesting that virion capture activity is associated with the Δ5G-specific linear epitope Ab (Fig. 7a). By contrast, IgG fractions from SIV239-infected animals collected at 3–4 weeks p.i. did not exhibit appreciable binding activity either to Δ5G virions or SIV239 virions (Fig. 7b). Thus, these results demonstrated that Δ5G infection elicited not only nAb after 8 weeks p.i., but also a much earlier humoral antiviral mechanism in the form of Δ5G-specific virion-binding Ab at 3–4 weeks p.i. in at least two monkeys (Mm07 and Mm22). To examine the relationship between the two antibody activities, we calculated the correlation of virion capture activity of IgG at 3 or 4 weeks p.i. with a peak nAb titre in Δ5G-infected animals (Fig. 2b) and found that this correlation was statistically significant ($r=1$, $P=0.0167$; Fig. 7c).

DISCUSSION

nAb response in Δ5G-infected animals

Glycosylation of viral spikes has long been recognized as an effective strategy to evade host (humoral) immune surveillance for several pathogens and for HIV/SIV in particular (Dowling *et al.*, 2007; Fournillier *et al.*, 2001; Haigwood & Stamatatos, 2003; Huso *et al.*, 1988; Reitter *et al.*, 1998). In support of these observations, the data presented here demonstrated that quintuple deglycosylation conferred live attenuated vaccine properties to an SIV239 mutant, Δ5G (Mori *et al.*, 2001); however, a cellular but not humoral response was detected as an immune correlate of the protection of Δ5G-infected animals against SIV239 challenge infection. Therefore, we assumed that the complete control of robust acute virus replication in Δ5G-infected animals beyond the initial cell-mediated control would be due to the development of rapid and effective nAbs. This study indicated that, whereas

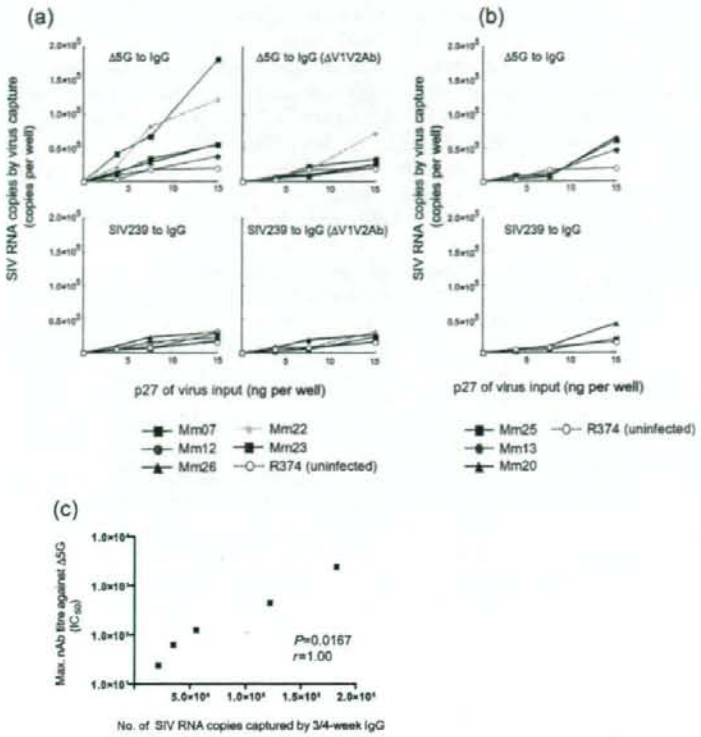

Fig. 7. Virion capture activity of IgG from Δ5G-infected and SIV239-infected animals. Virion capture activity of IgG from the plasma of infected animals at 3 or 4 weeks p.i. was determined by increased captured SIV RNA relative to input (3.75, 7.5 and 15 ng $p27^{gag}$) of Δ5G or SIV239. Plasma samples of Δ5G-infected animals (a) and SIV239-infected animals (b) were used for the assay. IgG (ΔV1V2Ab) indicates IgG depleted of Ab binding to V1V2-9, -10 or -11 peptide. R374 was an uninfected monkey. Correlation between virion capture activity at 3 or 4 weeks p.i. and peak nAb titre in Δ5G-infected animals (Fig. 2b) is shown (c).

Δ5G-infected animals clearly exhibited better nAb responses than SIV239-infected animals, the most stringent nAb assay, based on 90 % inhibition, provided evidence of nAb titres in only two of five Δ5G-infected animals and the appearance of these titres trailed the decline of acute viral loads by almost 4 weeks (Figs 1 and 2). Therefore, we concluded that, although deglycosylation did promote better development of nAbs in Δ5G-infection than SIV239 infection, it was still too late to control acute viraemia.

Zinkernagel and co-workers have categorized viruses into two types: 'acutely cytopathic viruses' and 'poorly or non-cytopathic viruses' (Hangartner *et al.*, 2006b). The former contains viruses such as vesicular stomatitis virus in mice and influenza virus in humans, whose control depends primarily on a rapid and potent nAb response. The latter comprises viruses such as lymphocytic choriomenigitis virus in mice, and hepatitis B and C viruses and HIV in humans, against which a nAb response is apparent only following the reduction of primary viraemia, and which establish persistent chronic infections. Accordingly, although the viral loads in Δ5G infection resembled 'acutely cytopathic virus' infections, the kinetics of nAbs still conformed to the 'non-cytopathic virus' category. As the difference in nAb response between the two types of virus is determined by their surface glycoproteins (Pinschewer *et al.*, 2004), this study suggests that the deglycosylation of Δ5G could not change this intrinsic property of SIV239.

Ab responses to Env peptides in Δ5G-infected animals

Aside from nAb, non-nAb responses to linear epitopes in V1/V2 were specifically induced by 3 weeks p.i. in all Δ5G-infected animals (Figs 4, 5 and 6). The heavy glycosylation of viral spikes clearly prevented access of B-cell receptors to the linear Ab epitopes located within limited regions of gp120 in SIV239, and the reduced glycosylation probably promoted better exposure of these linear epitopes in Δ5G (Fig. 4). Accordingly, the Δ5G-specific epitope in V1/V2 should be closely associated with the deglycosylation mutation at aa 171 in gp120 (Fig. 5). We speculate that this Ab induction might contribute to acute viral suppression in Δ5G infection because of the coincident decrease in peak viraemia (Figs 1 and 6). Non-neutralizing Abs can be divided into those that bind to the intact virion surface and debris-specific Ab. The former non-neutralizing Abs have occasional possibilities for antiviral activities such as antibody-dependent cell-mediated cytotoxicity and complement-mediated virus inactivation (Aasa-Chapman *et al.*, 2005; Ahmad & Menezes, 1996; Forthal *et al.*, 2001; Hangartner *et al.*, 2006a). In fact, readily detectable virion

capture Abs were induced in two of five Δ5G-infected animals (Fig. 7, Mm07 and Mm22). The importance of immediate-early suppression of SIV replication for the long-term containment of infection has been demonstrated by studies of post-exposure anti-retroviral therapy (Lifson *et al.*, 2000; Mori *et al.*, 2000). Thus, the early and complete control of viraemia in Δ5G-infected animals clearly suggests an antiviral mechanism(s) acting as early as 2–4 weeks p.i. Therefore, the early detection of IgG capable of virus capture in Δ5G-infected animals may provide mechanisms capable of contributing to undetectable viral load set points (Fig. 1b). The selective generation of such Ab directed to linear Env epitopes is expected.

Interestingly, deglycosylation in gp120 was also associated with a general reduction in the antigenicity of linear epitopes in gp41: the Ab response against the two epitopes that reside in the regions between the two heptad repeats (aa 601–625) and in the C-terminal heptad repeat (aa 660–685), respectively, was markedly reduced (Fig. 4, Table 1). The former corresponds to the highly conserved immunogenic epitope (Benichou *et al.*, 1993; Gnann *et al.*, 1987; Silvera *et al.*, 1994), and the latter corresponds to an epitope identified in the chronic phase of SIVmac251 infection (Silvera *et al.*, 1994) and corresponds to the nAb epitope of HIV-1 known as 2F5 (Muster *et al.*, 1993), although this linear epitope has not been associated with SIV neutralization (Caffrey *et al.*, 1998). Thus, these epitopes are probably exposed on the surface of viral spikes or their degraded fragments in most SIV and HIV-1 isolates with appropriate glycosylation and correct folding. We believe that the loss of glycosylation might induce a slight conformational change in the gp120 protein backbone, resulting in altered interaction of gp120 and gp41. In fact, the region encompassing the former epitope in gp41 was demonstrated to interact with gp120 (Cao *et al.*, 1993; Maerz *et al.*, 2001; York & Nunberg, 2004). As viral spikes determine virus properties such as viral receptor usage and cell tropism (Kolchinsky *et al.*, 2001; Puffer *et al.*, 2002), different cell populations might be infected in Δ5G-infected animals compared with SIV239 infection. More specifically, because of the distinct properties of the virus, vigorous Δ5G replication in the acute phase did not apparently impair immune function and thus established the control of chronic-phase infection and viral replication.

Host factors required for functional Ab responses against SIV infection

This study also demonstrated remarkable differences in humoral response with regard to nAb and virion capture Ab among Δ5G-infected animals. However, gp120-specific-binding Ab and the linear epitope-specific Ab were initially induced similarly in all animals. These findings imply that Abs measured by ELISA assay and Abs exhibiting antiviral activity are elicited by different pathways and that the properties associated with functional Abs depend largely on the host and underscore the importance of its genetic background. Rhesus macaques are present in various geographical locations within the Asian continent and are subdivided into many subspecies morphologically and genetically (Smith & McDonough, 2005). Some of the genetic differences among rhesus monkeys of different geographical origins, and especially those involving major histocompatibility complex (MHC) genotypes, probably influence the corresponding differences in immune responses, especially cellular response (Bontrop *et al.*, 1996; O'Connor *et al.*, 2003; Reimann *et al.*, 2005). Schmitz *et al.* (2005) reported that Mamu-A*01-positive rhesus monkeys elicited a significantly higher cellular response and lower nAb titres than those in Mamu-A*01-negative animals at the time of challenge infection of animals vaccinated with live attenuated SIV. They suggested that both humoral and cellular immune responses contributed to the protection against the challenge infection and that the relative contribution of each of the responses may be genetically determined. We observed a similar relationship between nAb and cellular responses among Δ5G-infected animals: two animals (Mm07 and Mm22) elicited a lower cellular response while the other three animals (Mm12, Mm23 and Mm26) elicited a higher cellular response (data not shown). Notably two animals exhibiting highly functional Ab (Mm07 and Mm22) were the offspring of seed animals imported from Laos, whilst the others (Mm12, Mm23 and Mm26) were of Burmese origin, suggesting the potential association of such different humoral and cellular responses with host genetic factors. In clinical studies, considerable concordance of adaptive cellular and humoral responses and HIV evolution in monozygotic twins, but not in brothers, infected with the same virus has been reported (Draenert *et al.*, 2006). HIV-1-exposed but uninfected status with significantly higher neutralizing IgA was linked to genotypes on chromosome 22 (Kanari *et al.*, 2005). In the mouse Friend leukemia virus model, MHC II alleles were determined as host genetic factors required for effective nAb response (Miyazawa *et al.*, 1992) and the host genetic factor was mapped to chromosome 15, which was associated with the clearance of viraemia by nAb (Hasenkrug *et al.*, 1995; Kanari *et al.*, 2005).

Taken together, we speculate that the functional humoral response is determined by host genetic properties similar to the cellular immune response. Thus, gaining knowledge of the genetic requirements for both humoral and cellular containment of viral infections will clearly be of primary importance for vaccine development and therapeutics against HIV and other infectious agents.

NOTE ADDED IN PROOF

A discrepancy in the SIV239-infected animals Mm13 and Mm20 was noted between the result shown in Fig. 2 and that in a previous report Mori *et al.*, 2001. The nAb

response against SIV239 in Mm20 was confirmed at multiple time points in the present study.

ACKNOWLEDGEMENTS

We thank Kayoko Ueda for excellent technical assistance and Marcelo Kuroda for critical reading of the manuscript. This study was conducted through the Cooperative Research Program in the Tsukuba Primate Research Center, National Institute of Biomedical Innovation, Japan. This work was supported by AIDS research grants from the Health Sciences Research Grants, from the Ministry of Health, Labour and Welfare in Japan, and from the Ministry of Education, Culture, Sports, Science and Technology in Japan.

REFERENCES

Aasa-Chapman, M. M., Holuigue, S., Aubin, K., Wong, M., Jones, N. A., Cornforth, D., Pellegrino, P., Newton, P., Williams, I. & other authors (2005). Detection of antibody-dependent complement-mediated inactivation of both autologous and heterologous virus in primary human immunodeficiency virus type 1 infection. *J Virol* **79**, 2823–2830.

Ahmad, A. & Menezes, J. (1996). Antibody-dependent cellular cytotoxicity in HIV infections. *FASEB J* **10**, 258–266.

Benichou, S., Venet, A., Beyer, C., Tiollais, P. & Madaule, P. (1993). Characterization of B-cell epitopes in the envelope glycoproteins of simian immunodeficiency virus. *Virology* **194**, 870–874.

Bontrop, R. E., Otting, N., Niphuis, H., Noort, R., Teeuwsen, V. & Heeney, J. L. (1996). The role of major histocompatibility complex polymorphisms on SIV infection in rhesus macaques. *Immunol Lett* **51**, 35–38.

Burns, D. P. & Desrosiers, R. C. (1991). Selection of genetic variants of simian immunodeficiency virus in persistently infected rhesus monkeys. *J Virol* **65**, 1843–1854.

Burton, D. R., Desrosiers, R. C., Doms, R. W., Koff, W. C., Kwong, P. D., Moore, J. P., Nabel, G. J., Sodroski, J., Wilson, I. A. & Wyatt, R. T. (2004). HIV vaccine design and the neutralizing antibody problem. *Nat Immunol* **5**, 233–236.

Caffrey, M., Cai, M., Kaufman, J., Stahl, S. J., Wingfield, P. T., Covell, D. G., Gronenborn, A. M. & Clore, G. M. (1998). Three-dimensional solution structure of the 44 kDa ectodomain of SIV gp41. *EMBO J* **17**, 4572–4584.

Cao, J., Bergeron, L., Helseth, E., Thali, M., Repke, H. & Sodroski, J. (1993). Effects of amino acid changes in the extracellular domain of the human immunodeficiency virus type 1 gp41 envelope glycoprotein. *J Virol* **67**, 2747–2755.

Chackerian, B., Rudensey, L. M. & Overbaugh, J. (1997). Specific *N*-linked and *O*-linked glycosylation modifications in the envelope V1 domain of simian immunodeficiency virus variants that evolve in the host alter recognition by neutralizing antibodies. *J Virol* **71**, 7719–7727.

Chen, B., Vogan, E. M., Gong, H., Skehel, J. J., Wiley, D. C. & Harrison, S. C. (2005). Structure of an unliganded simian immunodeficiency virus gp120 core. *Nature* **433**, 834–841.

Cheng-Mayer, C., Brown, A., Harouse, J., Luciw, P. A. & Mayer, A. J. (1999). Selection for neutralization resistance of the simian/human immunodeficiency virus $SHIV_{SF33A}$ variant in vivo by virtue of sequence changes in the extracellular envelope glycoprotein that modify *N*-linked glycosylation. *J Virol* **73**, 5294–5300.

Choi, W. S., Collignon, C., Thiriart, C., Burns, D. P., Stott, E. J., Kent, K. A. & Desrosiers, R. C. (1994). Effects of natural sequence variation on recognition by monoclonal antibodies neutralize simian immunodeficiency virus infectivity. *J Virol* **68**, 5395–5402.

Dowling, W., Thompson, E., Badger, C., Mellquist, J. L., Garrison, A. R., Smith, J. M., Paragas, J., Hogan, R. J. & Schmaljohn, C. (2007). Influences of glycosylation on antigenicity, immunogenicity, and protective efficacy of Ebola virus GP DNA vaccines. *J Virol* **81**, 1821–1837.

Draenert, R., Allen, T. M., Liu, Y., Wrin, T., Chappey, C., Verrill, C. L., Sirera, G., Eldridge, R. L., Lahaie, M. P. & other authors (2006). Constraints on HIV-1 evolution and immunodominance revealed in monozygotic adult twins infected with the same virus. *J Exp Med* **203**, 529–539.

Eberle, J., Loussert-Ajaka, I., Brust, S., Zekeng, L., Hauser, P. H., Kaptue, L., Knapp, S., Damond, F., Saragosti, S. & other authors (1997). Diversity of the immunodominant epitope of gp41 of HIV-1 subtype O and its validity for antibody detection. *J Virol Methods* **67**, 85–91.

Forthal, D. N., Landucci, G. & Keenan, B. (2001). Relationship between antibody-dependent cellular cytotoxicity, plasma HIV type 1 RNA, and $CD4^+$ lymphocyte count. *AIDS Res Hum Retroviruses* **17**, 553–561.

Fournillier, A., Wychowski, C., Boucreux, D., Baumert, T. F., Meunier, J. C., Jacobs, D., Muguet, S., Depla, E. & Inchauspe, G. (2001). Induction of hepatitis C virus E1 envelope protein-specific immune response can be enhanced by mutation of *N*-glycosylation sites. *J Virol* **75**, 12088–12097.

Gnann, J. W., Jr, Nelson, J. A. & Oldstone, M. B. (1987). Fine mapping of an immunodominant domain in the transmembrane glycoprotein of human immunodeficiency virus. *J Virol* **61**, 2639–2641.

Haigwood, N. L. & Stamatatos, L. (2003). Role of neutralizing antibodies in HIV infection. *AIDS* **17** (Suppl. 4), S67–S71.

Hangartner, L., Zellweger, R. M., Giobbi, M., Weber, J., Eschli, B., McCoy, K. D., Harris, N., Recher, M., Zinkernagel, R. M. & Hengartner, H. (2006a). Nonneutralizing antibodies binding to the surface glycoprotein of lymphocytic choriomeningitis virus reduce early virus spread. *J Exp Med* **203**, 2033–2042.

Hangartner, L., Zinkernagel, R. M. & Hengartner, H. (2006b). Antiviral antibody responses: the two extremes of a wide spectrum. *Nat Rev Immunol* **6**, 231–243.

Hasenkrug, K. J., Valenzuela, A., Letts, V. A., Nishio, J., Chesebro, B. & Frankel, W. N. (1995). Chromosome mapping of *Rfv3*, a host resistance gene to Friend murine retrovirus. *J Virol* **69**, 2617–2620.

Hofmann-Lehmann, R., Swenerton, R. K., Liska, V., Leutenegger, C. M., Lutz, H., McClure, H. M. & Ruprecht, R. M. (2000). Sensitive and robust one-tube real-time reverse transcriptase-polymerase chain reaction to quantify SIV RNA load: comparison of one- versus two-enzyme systems. *AIDS Res Hum Retroviruses* **16**, 1247–1257.

Huso, D. L., Narayan, O. & Hart, G. W. (1988). Sialic acids on the surface of caprine arthritis-encephalitis virus define the biological properties of the virus. *J Virol* **62**, 1974–1980.

Johnson, W. E., Sanford, H., Schwall, L., Burton, D. R., Parren, P. W., Robinson, J. E. & Desrosiers, R. C. (2003). Assorted mutations in the envelope gene of simian immunodeficiency virus lead to loss of neutralization resistance against antibodies representing a broad spectrum of specificities. *J Virol* **77**, 9993–10003.

Kanari, Y., Clerici, M., Abe, H., Kawabata, H., Trabattoni, D., Caputo, S. L., Mazzotta, F., Fujisawa, H., Niwa, A. & other authors (2005). Genotypes at chromosome 22q12–13 are associated with HIV-1-exposed but uninfected status in Italians. *AIDS* **19**, 1015–1024.

Kent, K. A., Rud, E., Corcoran, T., Powell, C., Thiriart, C., Collignon, C. & Stott, E. J. (1992). Identification of two neutralizing and 8 non-neutralizing epitopes on simian immunodeficiency virus envelope

using monoclonal antibodies. *AIDS Res Hum Retroviruses* **8**, 1147–1151.

Kolchinsky, P., Kiprilov, E., Bartley, P., Rubinstein, R. & Sodroski, J. (2001). Loss of a single *N*-linked glycan allows CD4-independent human immunodeficiency virus type 1 infection by altering the position of the gp120 V1/V2 variable loops. *J Virol* **75**, 3435–3443.

Leonard, C. K., Spellman, M. W., Riddle, L., Harris, R. J., Thomas, J. N. & Gregory, T. J. (1990). Assignment of intrachain disulfide bonds and characterization of potential glycosylation sites of the type 1 recombinant human immunodeficiency virus envelope glycoprotein (gp120) expressed in Chinese hamster ovary cells. *J Biol Chem* **265**, 10373–10382.

Lifson, J. D., Rossio, J. L., Arnaout, R., Li, L., Parks, T. L., Schneider, D. K., Kiser, R. F., Coalter, V. J., Walsh, G. & other authors (2000). Containment of simian immunodeficiency virus infection: cellular immune responses and protection from rechallenge following transient postinoculation antiretroviral treatment. *J Virol* **74**, 2584–2593.

Liu, J., Wang, S., Hoxie, J. A., LaBranche, C. C. & Lu, M. (2002). Mutations that destabilize the gp41 core are determinants for stabilizing the simian immunodeficiency virus-CPmac envelope glycoprotein complex. *J Biol Chem* **277**, 12891–12900.

Maerz, A. L., Drummer, H. E., Wilson, K. A. & Poumbourios, P. (2001). Functional analysis of the disulfide-bonded loop/chain reversal region of human immunodeficiency virus type 1 gp41 reveals a critical role in gp120-gp41 association. *J Virol* **75**, 6635–6644.

Means, R. E., Greenough, T. & Desrosiers, R. C. (1997). Neutralization sensitivity of cell culture-passaged simian immunodeficiency virus. *J Virol* **71**, 7895–7902.

Miyazawa, M., Nishio, J., Wehrly, K. & Chesebro, B. (1992). Influence of MHC genes on spontaneous recovery from Friend retrovirus-induced leukemia. *J Immunol* **148**, 644–647.

Mori, K., Yasutomi, Y., Sawada, S., Villinger, F., Sugama, K., Rosenwith, B., Heeney, J. L., Uberla, K., Yamazaki, S. & other authors (2000). Suppression of acute viremia by short-term postexposure prophylaxis of simian/human immunodeficiency virus SHIV-RT-infected monkeys with a novel reverse transcriptase inhibitor (GW420867) allows for development of potent antiviral immune responses resulting in efficient containment of infection. *J Virol* **74**, 5747–5753.

Mori, K., Yasutomi, Y., Ohgimoto, S., Nakasone, T., Takamura, S., Shioda, T. & Nagai, Y. (2001). Quintuple deglycosylation mutant of simian immunodeficiency virus SIVmac239 in rhesus macaques: robust primary replication, tightly contained chronic infection, and elicitation of potent immunity against the parental wild-type strain. *J Virol* **75**, 4023–4028.

Mori, K., Sugimoto, C., Ohgimoto, S., Nakayama, E. E., Shioda, T., Kusagawa, S., Takebe, Y., Kano, M., Matano, T. & other authors (2005). Influence of glycosylation on the efficacy of an Env-based vaccine against simian immunodeficiency virus SIVmac239 in a macaque AIDS model. *J Virol* **79**, 10386–10396.

Muster, T., Steindl, F., Purtscher, M., Trkola, A., Klima, A., Himmler, G., Ruker, F. & Katinger, H. (1993). A conserved neutralizing epitope on gp41 of human immunodeficiency virus type 1. *J Virol* **67**, 6642–6647.

Nishimura, Y., Igarashi, T., Haigwood, N., Sadjadpour, R., Plishka, R. J., Buckler-White, A., Shibata, R. & Martin, M. A. (2002). Determination of a statistically valid neutralization titer in plasma that confers protection against simian-human immunodeficiency virus challenge following passive transfer of high-titered neutralizing antibodies. *J Virol* **76**, 2123–2130.

Nyambi, P. N., Gorny, M. K., Bastiani, L., van der Groen, G., Williams, C. & Zolla-Pazner, S. (1998). Mapping of epitopes exposed on intact human immunodeficiency virus type 1 (HIV-1) virions: a new strategy for studying the immunologic relatedness of HIV-1. *J Virol* **72**, 9384–9391.

O'Connor, D. H., Mothe, B. R., Weinfurter, J. T., Fuenger, S., Rehrauer, W. M., Jing, P., Rudersdorf, R. R., Liebl, M. E., Krebs, K. & other authors (2003). Major histocompatibility complex class I alleles associated with slow simian immunodeficiency virus disease progression bind epitopes recognized by dominant acute-phase cytotoxic-T-lymphocyte responses. *J Virol* **77**, 9029–9040.

Ohgimoto, S., Shioda, T., Mori, K., Nakayama, E. E., Hu, H. & Nagai, Y. (1998). Location-specific, unequal contribution of the *N* glycans in simian immunodeficiency virus gp120 to viral infectivity and removal of multiple glycans without disturbing infectivity. *J Virol* **72**, 8365–8370.

Pinschewer, D. D., Perez, M., Jeetendra, E., Bachi, T., Horvath, E., Hengartner, H., Whitt, M. A., de la Torre, J. C. & Zinkernagel, R. M. (2004). Kinetics of protective antibodies are determined by the viral surface antigen. *J Clin Invest* **114**, 988–993.

Puffer, B. A., Pohlmann, S., Edinger, A. L., Carlin, D., Sanchez, M. D., Reitter, J., Watry, D. D., Fox, H. S., Desrosiers, R. C. & Doms, R. W. (2002). CD4 independence of simian immunodeficiency virus Envs is associated with macrophage tropism, neutralization sensitivity, and attenuated pathogenicity. *J Virol* **76**, 2595–2605.

Regier, D. A. & Desrosiers, R. C. (1990). The complete nucleotide sequence of a pathogenic molecular clone of simian immunodeficiency virus. *AIDS Res Hum Retroviruses* **6**, 1221–1231.

Reimann, K. A., Parker, R. A., Seaman, M. S., Beaudry, K., Beddall, M., Peterson, L., Williams, K. C., Veazey, R. S., Montefiori, D. C. & other authors (2005). Pathogenicity of simian-human immunodeficiency virus SHIV-89.6P and SIVmac is attenuated in cynomolgus macaques and associated with early T-lymphocyte responses. *J Virol* **79**, 8878–8885.

Reitter, J. N., Means, R. E. & Desrosiers, R. C. (1998). A role for carbohydrates in immune evasion in AIDS. *Nat Med* **4**, 679–684.

Schmitz, J. E., Johnson, R. P., McClure, H. M., Manson, K. H., Wyand, M. S., Kuroda, M. J., Lifton, M. A., Khunkhun, R. S., McEvers, K. J. & other authors (2005). Effect of $CD8^+$ lymphocyte depletion on virus containment after simian immunodeficiency virus SIVmac251 challenge of live attenuated SIVmac239Δ3-vaccinated rhesus macaques. *J Virol* **79**, 8131–8141.

Silvera, P., Flanagan, B., Kent, K., Rud, E., Powell, C., Corcoran, T., Bruck, C., Thiriart, C., Haigwood, N. L. & Stott, E. J. (1994). Fine analysis of humoral antibody response to envelope glycoprotein of SIV in infected and vaccinated macaques. *AIDS Res Hum Retroviruses* **10**, 1295–1304.

Smith, D. G. & McDonough, J. (2005). Mitochondrial DNA variation in Chinese and Indian rhesus macaques (*Macaca mulatta*). *Am J Primatol* **65**, 1–25.

Wei, X., Decker, J. M., Wang, S., Hui, H., Kappes, J. C., Wu, X., Salazar-Gonzalez, J. F., Salazar, M. G., Kilby, J. M. & other authors (2003). Antibody neutralization and escape by HIV-1. *Nature* **422**, 307–312.

Wyatt, R. & Sodroski, J. (1998). The HIV-1 envelope glycoproteins: fusogens, antigens, and immunogens. *Science* **280**, 1884–1888.

Wyatt, R., Kwong, P. D., Desjardins, E., Sweet, R. W., Robinson, J., Hendrickson, W. A. & Sodroski, J. G. (1998). The antigenic structure of the HIV gp120 envelope glycoprotein. *Nature* **393**, 705–711.

York, J. & Nunberg, J. H. (2004). Role of hydrophobic residues in the central ectodomain of gp41 in maintaining the association between human immunodeficiency virus type 1 envelope glycoprotein subunits gp120 and gp41. *J Virol* **78**, 4921–4926.

Yu, D., Shioda, T., Kato, A., Hasan, M. K., Sakai, Y. & Nagai, Y. (1997). Sendai virus-based expression of HIV-1 gp120: reinforcement by the V(−) version. *Genes Cells* **2**, 457–466.

Zhang, M., Gaschen, B., Blay, W., Foley, B., Haigwood, N., Kuiken, C. & Korber, B. (2004). Tracking global patterns of *N*-linked glycosylation site variation in highly variable viral glycoproteins: HIV, SIV, and HCV envelopes and influenza hemagglutinin. *Glycobiology* **14**, 1229–1246.

Zolla-Pazner, S. (2004). Identifying epitopes of HIV-1 that induce protective antibodies. *Nat Rev Immunol* **4**, 199–210.

J Neuropathol Exp Neurol

Vol. 67, No. 6
June 2008
pp. 600–611

ORIGINAL ARTICLE

Impaired Astrocytes and Diffuse Activation of Microglia in the Cerebral Cortex in Simian Immunodeficiency Virus-Infected Macaques Without Simian Immunodeficiency Virus Encephalitis

Hui Qin Xing, MD, PhD, Kazuyasu Mori, PhD, Chie Sugimoto, PhD, Fumiko Ono, PhD, Kimiko Izumo, MA, Ryuji Kuboda, MD, PhD, and Shuji Izumo, MD, PhD

Abstract

Various types of neuronal damage have been reported in acquired immunodeficiency syndrome (AIDS) dementia. We previously demonstrated that inflammation and cortical damage occur independently according to viral tropism in a simian immunodeficiency virus (SIV)-infected macaque model of AIDS dementia. To elucidate the pathogenesis of cortical degeneration, we examined the frontal cortex of SIV-infected macaques and found apoptosis and decreased expression of the excitatory amino acid transporter 2 in astrocytes and diffuse activation of microglia in association with limited neuronal damage. Some activated microglia also expressed excitatory amino acid transporter 2 but not proinflammatory cytokines. No inflammatory changes were seen in the cortex or the white matter, and SIV-infected cells were not detected in or around cortical lesions either by immunohistochemistry or by the polymerase chain reaction detection of SIV genomes of extracted DNA from microdissected tissue samples. These results indicate that an astrocytic abnormality and a compensatory activation of microglia might provide a protective effect against neuronal degeneration in the frontal cortex of SIV-infected macaques without SIV encephalitis.

Key Words: AIDS encephalopathy, Animal model, Cerebral cortex, Immunohistochemistry, Injury of astrocytes, Neuroprotection by microglia

INTRODUCTION

Human immunodeficiency virus 1 (HIV-1) can induce acquired immunodeficiency syndrome dementia complex (ADC), a clinical triad of progressive cognitive decline, motor dysfunction, and behavioral abnormalities, which eventually affects 15% to 20% of AIDS patients (1, 2). Although the introduction of highly active anti-retroviral therapy has reduced progression of AIDS, inconsistent results have been reported regarding the effects of highly active antiretroviral therapy on central nervous system (CNS) involvement (3–8), thus suggesting that the prevalence of dementia may eventually increase corresponding to longer life spans of people with HIV-1 infection.

One of the histopathologic correlates of ADC is diffuse and nodular inflammatory infiltrates with formation of multinucleated giant cells (MNGCs) in the brain white matter (9, 10). Myelin pallor (11) and axonal damage (12–14) with abundant HIV-1-infected macrophages and microglia have been mainly demonstrated in the white matter (15, 16), but poor correlations between these findings and the clinical manifestations of ADC have been repeatedly reported (17, 18). On the other hand, Budka et al (10, 11) described astrocytic gliosis, a reduction of neurons and proliferation of rod cells in the cerebral cortex of many cases with HIV-1 infection and have identified this diffuse poliodystrophy (DPD) as an additional histopathologic feature of ADC. Furthermore, a variety of pathologic findings, including neuronal loss (19–21), apoptosis (22), and synaptic and dendritic simplification (23–25), have been reported in the cortex in HIV-AIDS. Because of the complexity of the histopathologic findings in human autopsy brains, however, a precise relationship between these histopathologic changes, namely, the inflammatory process in the white matter and degenerative process in the cortex, has not been elucidated.

Simian immunodeficiency virus (SIV) infection in rhesus macaques is considered to be a suitable animal model of human HIV-1 infection and has been used in various studies as a model for AIDS encephalopathy. Desrosiers et al (26) reported that macrophage-tropic variants of SIV were associated with the appearance of encephalitis. Previously, we inoculated macaques with 3 SIV strains and investigated the relationship between the lymph node and brain pathology. The animals infected with macrophage virus tropic-SIV239env/MERT chymeric virus, did not develop AIDS 3 to 4 years after infection, but microglial nodules with MNGCs were demonstrated in the white matter, and no pathologic changes were noticed in the cerebral cortex. The other animals infected with T-cell-tropic viruses SIVmac239 and SIV/HIV-1-(SHIV)-RT

From the Division of Molecular Pathology (XHQ, KI, RK, SI), Center for Chronic Viral Diseases, Graduate School of Medical and Dental Sciences, Kagoshima University, Kagoshima; AIDS Research Center (KM, CS), National Institute of Infectious Diseases, Shinjuku-ku, Tokyo and Tsukuba Primate Research Center, National Institute of Biomedical Innovation; and Corporation for Production and Research of Laboratory Primates (FO), Tsukuba, Ibaraki, Japan.

Send correspondence and reprint requests to: Shuji Izumo, MD, PhD, Division of Molecular Pathology, Center for Chronic Viral Diseases, Graduate School of Medical and Dental Sciences, Kagoshima University, 8-35-1 Sakuragaoka, Kagoshima 890-8544, Japan; E-mail: izumo@m.kufm.kagoshima-u.ac.jp

This work was supported by AIDS research grants from the Health Sciences Research Grants from the Ministry of Health, Labour, and Welfare in Japan.

developed typical simian AIDS pathology in the lymph nodes within 3 years after infection; the cerebral cortex of these animals showed astrocytic gliosis and electron microscopic abnormalities without evidence of microglial nodules or MNGCs in the white matter. From these observations, we hypothesized that there are 2 independent pathogenetic processes in simian AIDS encephalopathy, that is, immune response against virus-infected macrophage/microglial cells in the white matter without immunodeficiency and cortical degeneration caused in the late stage of AIDS (27).

The roles of macrophage infiltration and microglial activation in the pathogenesis of HIV encephalitis have been extensively studied. With respect to the cortical pathology, the expression of viral neurotoxins or neurotoxic cytokines from microglia and/or astrocytes has been reported to induce neuronal dysfunction and death (28–31). On the other hand, recent reports suggest that activated microglia express excitatory amino acid transporters (EAATs) and glutamine synthetase, and may be neuroprotective in the early stages of the disease (32, 33). In our SIV model, degenerative changes were observed in the cerebral cortex of macaques infected with T-cell-tropic viruses, and microglial nodules with MNGCs were absent (27); therefore, we further examined the frontal cortex of rhesus macaques infected with T-lymphocyte-tropic SIV and focused on microglial activation, apoptosis, and EAAT-2 expression, as well as localization of virus-infected cells.

MATERIALS AND METHODS

Virus

Molecularly cloned SIVmac239 is a T-lymphocyte-tropic virus, the pathogenic properties of which have been previously described. This virus causes immunosuppression and eventually leads to the development of AIDS in macaques. A chimeric virus, SHIV-RT, consists of a SIVmac239 virus backbone in which the *SIV RT* gene was replaced by the HIV-1 *HxB2 RT* gene, as previously described (27, 34). In experimentally infected rhesus monkeys, SHIV-RT has been shown to induce AIDS (34, 35).

Animals

Eleven rhesus macaques were screened and found to be seronegative for SIV, simian T-lymphotropic virus, B virus, and Type D retroviruses. Four macaques (532, 627, 682, and 730) were inoculated intravenously with SIVmac239 and killed 133, 46, 115, and 463 weeks after inoculation, respectively. The other 3 (631, 677, and 700) were inoculated with SHIV-RT and killed 108, 156, and 263 weeks after inoculation, respectively. Four uninfected macaques (671, 630, 778, and 780) were used as controls (Table 1). The animals were housed in individual cages and maintained according to the rules and guidelines of the National Institute for Infectious Diseases for experimental animal welfare. The animals were killed at various times after infection when they became moribund.

$CD4^+$ Cell Counts and Viral RNA Loads

$CD4^+$ cell counts were performed on peripheral blood samples at the time of autopsy. To measure the level of virus replication in the periphery, viral RNA was quantified in plasma at autopsy. Viral RNA in the plasma of inoculated macaques was measured by real-time reverse transcriptase-polymerase chain reaction (PCR).

Histopathology and Immunohistochemistry

The routine histopathologic methods used in this study have been described elsewhere (27). Brain tissue specimens were embedded in paraffin, sectioned, and mounted on glass slides. The EnVision system (DAKO, Carpinteria, CA) was used for immunohistochemistry except for a guinea pig anti-glial glutamate transporter 1, EAAT-2 antibody with which the avidin-biotin-peroxidase complex method (Vector, Burlingame, CA) was applied. Immunoreactivity was visualized using either diaminobenzidine/peroxidase (brown) or the 3-amino-9-ethyl-carbazole substrate-chromogen system (DAKO; red). Light counterstaining was done with hematoxylin.

TABLE 1. Clinical Data

Animal No.	Sex	Age at Virus Inoculation, weeks	Age at Death, weeks	Duration of Infection, weeks	Viral Inocula	Viral RNA Load in Plasma at Autopsy, copies/ml	$CD4^+$ Cell Count in PBMCs at Autopsy, per μl	Clinical Information
532	M	260	393	133	SIVmac239	214,300	380	Weight loss and moribund
627	M	312	358	46	SIVmac239	25,000	90	Weight loss and moribund
682	M	100	215	115	SIVmac239	480,000	140	Weight loss and self-biting
730	M	156	619	463	SIVmac239	67,000	275	Weight loss and moribund
631	F	156	264	108	SHIV-RT	2,500,000	200	Weight loss and inactivity, inguinal B-cell lymphoma
677	M	104	260	156	SHIV-RT	6,900	100	Weight loss and moribund
700	M	104	367	263	SHIV-RT	530,000	192	Weight loss and moribund
630					Control			
671					Control			
778					Control			
780					Control			

PBMC, peripheral blood mononuclear cell; SHIV, simian immunodeficiency virus/human immunodeficiency virus-1.

Antibodies

To identify activated microglia, we used a mouse monoclonal antibody to human macrophage CD68 (KP1, 1:50; DAKO) and a rabbit anti-ionized calcium-binding adaptor molecule 1 antibody (Iba1; 1:500; Wako Chemicals, Osaka, Japan) (36). To characterize astrocyte abnormalities, we used a guinea pig anti-glial glutamate transporter 1, EAAT-2 antibody (1:6000; Chemicon, Temecula, CA). For SIV-infected cells, we used an anti-SIV envelope gp160/gp32 antibody (KK41; 1:50; Dr K. Kent and the National Institute for Biological Standards and Control), which has been previously described (27). Lymph nodes of SIV-infected and uninfected animals were used as positive and negative controls, respectively.

A mouse anti-human Ki-67 antibody (1:300; DAKO) that can detect cells in all active phases (G1, S, G2, and M) of the cell cycle was used to detect dividing cells. Sections of lymph nodes and small intestines were used as positive controls for proliferating cells. A mouse anti-human tumor necrosis factor antibody (TNF-α; 1:400; Abcam, Cambridge, MA) and a rabbit polyclonal antibody against interleukin 1β (IL-1β; 1:200; Santa Cruz Biotechnology, Santa Cruz, CA) were used to detect the respective cytokines. A tonsil with chronic inflammation was used as a positive control. We also performed glial fibrillary acidic protein (GFAP), CD3, and CD20 immunohistochemical staining for routine cell characterization.

Double Label Immunohistochemistry

Double label immunohistochemistry was performed for GFAP or Iba1 and Ki-67 to determine the phenotype of the proliferating cells by first performing immunohistochemistry for Iba1 or GFAP using the EnVision system (DAKO) and then for Ki-67 using avidin-biotin-peroxidase complex (Vector). Double labeling was performed using diaminobenzidine/peroxidase, followed by Vector blue/alkaline phosphatase. We also performed fluorescence microscopy for double label staining of EAAT-2 and Iba1 using fluorescein isothiocyanate and rhodamine-based detection methods.

Apoptosis

In situ terminal deoxynucleotidyl transferase-mediated dUTP-biotin end labeling of fragmented DNA (TUNEL) was done using the ApopTag in situ apoptosis detection kit (Chemicon). We also performed immunohistochemistry using an affinity-purified polyclonal rabbit immunoglobulin G directed specifically against the active form of caspase 3 (1:1000; R and D Systems, Minneapolis, MN) and anti-single-stranded DNA antibody (ssDNA; 1:250; DakoCytomation, Kyoto, Japan) for the identification of apoptotic cells. Lymph nodes and small intestines were used as positive controls. To examine the phenotype of apoptotic cells, we performed double label immunohistochemistry for GFAP and activated caspase 3 or ssDNA using the same method.

Electron Microscopy

Pieces of the frontal cortex from animals 531, 627, 682, and 630 were postfixed in 1% osmium tetroxide and embedded in epoxy resin. One-micrometer semithin sections of Epon-embedded samples were stained with toluidine blue and safranine. For electron microscopy, sections were stained with uranium acetate and lead citrate and examined using a Hitachi H-7000 electron microscope.

Quantitative and Semiquantitative Analysis

Ionized calcium-binding adaptor molecule 1 antibody-positive cells were counted in 10 200×-magnified light microscopic fields of cortical layers 2 to 5 of the middle frontal gyrus. These findings were considered to indicate an increase in the activated microglia when more than 700 Iba1-positive cells were counted in these 10 fields. We also performed semiquantitative assessments for the following immunohistochemical findings: astrocytic gliosis, EAAT-2 expression, Ki-67 or CD68-positive cells, TNF-α, and IL-1β expression.

Laser Microdissection and PCR-Based Detection of *SIV gag* and *SIV env* Genes

Polymerase chain reaction-based molecular detection of SIV genomes was performed to detect SIV-infected cells in the brain lesions of SIV-infected animal 532, which showed representative clinical and pathologic features. Paraffin-embedded sections of the frontal lobe were dehydrated, stained with hematoxylin, and air-dried. The parenchyma of the frontal cortex, perivascular areas of the frontal cortex, and white matter were identified based on cellular staining patterns and separately dissected using a laser microdissection system (AS LMD; Leica, Wetzlar, Germany). From each dissected sample, genomic DNA was extracted by a DNeasy tissue handbook kit (Qiagen, Tokyo, Japan). We used 2 sets of nested oligonucleotide primer pairs for the PCR detection of SIV provirus (37). The sequences of the primer

TABLE 2. Oligonucleotides Used as Primers in Nested PCR to Detect SIV gag and SIV env Proteins

Region of Amplification	Sequence of Outer Primers	Sequence of Inner Primers
SIV gag	5′-ACTGTCTGCGTCATCTGGTGC	5′-CACGCAGAAAAAGTGAAAC
	5′-GTCCCAATCTGCAGCCTCCTC	5′-CTCTGATAATCTGCATAGCCGC
SIV env	5′-TTATGGTGTACCAGCTTGGAGGAATGC	5′-CGATACTTGGGGAACAACTCAGTGCCTAC
	5′-CCAAACCAAGTAGAAGTCTGTGTCTCCATC	5′-GAGACCACCACCTTAGAACATTTAGGC
β-Globin	3′-TCCCAGTTTCTCCAGTTTCC	
	3′-AGACCATCCTGGCTAACACG	

PCR, polymerase chain reaction; SIV, simian immunodeficiency virus.

pairs used to detect SIV gag, SIV env, and β-globin as genomic control are listed in Table 2. The relative detection efficiency of all the primer sets was determined in a series of preliminary experiments. The DNA from SIV plasmid and paraffin sections of lymph node from SIVmac239-infected macaque 682 with abundant SIV-Env-positive cells was amplified as positive controls, and DNA from a lymph node of uninfected macaque 671 was amplified as a negative control in all assays to monitor potential PCR contamination. Each cycle consisted of 1 minute denaturation at 94°C, 1 minute primer annealing at 55°C, and 1 minute extension at 72°C. After 30 cycles, 4 ml of the amplified DNA was taken, and 30 additional cycles of amplification were carried out using the nested primers. The same primers for β-globin were used in a second PCR. After the second round of amplification, a 13-μl aliquot of the reaction products was applied for 2% agarose gel electrophoresis and visualized by ethidium bromide staining.

RESULTS

Clinical Manifestations

Table 1 summarizes the clinical data, including the viral RNA loads and $CD4^+$ cell counts in the peripheral blood, at the time of autopsy from the 7 SIV-infected rhesus macaques. Among the 4 macaques infected with SIVmac239, macaque 627 showed the most rapid decrease in the $CD4^+$ cell counts and became moribund within 46 weeks after infection. Macaque 532 had a prolonged clinical course and showed very high viral loads and decreased $CD4^+$ cell counts at 133 weeks after infection; thereafter, it became moribund and was diagnosed to have AIDS because of very low $CD4^+$ CD29 high T cells (less than 1% of peripheral blood mononuclear cells). Macaque 682 also had a prolonged clinical course and showed very high viral loads and decreased $CD4^+$ cell counts. This animal was killed for autopsy 115 weeks after infection because of self-biting

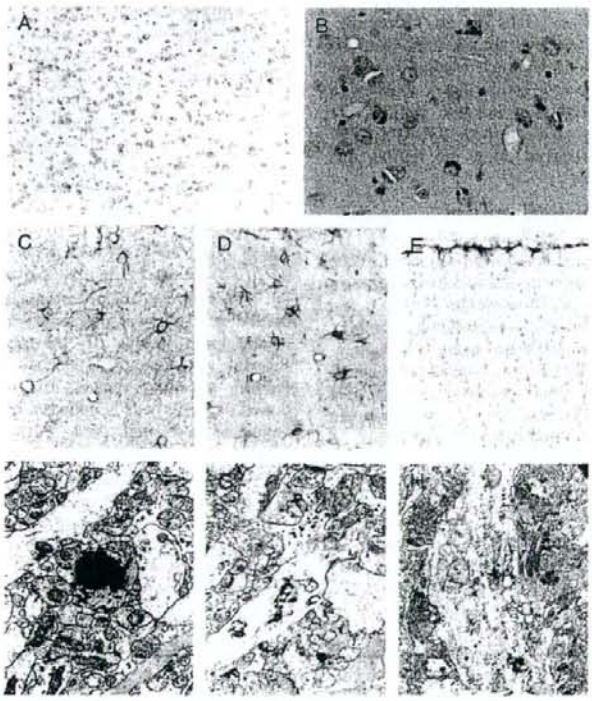

FIGURE 1. Representative findings in the frontal cortex of simian immunodeficiency virus (SIV)-infected macaques. Loss of neurons is not apparent **(A)**, but there is an increase in small glial cells and satellitosis around neurons **(B)** in a SIVmac239-infected macaque. Diffuse gliosis in SIVmac239-infected macaque **(C)** and in a SIV/human immunodeficiency virus-1-RT-infected macaque **(D)** contrasts with the uninfected control **(E)**. By electron microscopy, in the SIVmac239-infected macaque, there is deposition of glycogen-like granules **(F)** and an increase in lamellar bodies in the dendrites **(G)**. Foamy changes are detected in the cytoplasm of dendritic trunks **(H)**. Some astrocyte processes contain glial fibrils **(F, G)**. **(A)** Klüver-Barrera; **(B)** hematoxylin and eosin; **(C–E)**: anti-glial fibrillary acidic protein immunohistochemistry; **(F–H)** Electron microscopy. Original magnifications: **(A, E)** 100×; **(B)** 200×; **(C, D)** 400×; **(F)** 9,000×; **(G)** 15,000×; **(H)** 9,000×. **(A, B, F, G)** from macaque 627; **(C)** from macaque 532; **(D)** from macaque 631; **(E)** from macaque 630.

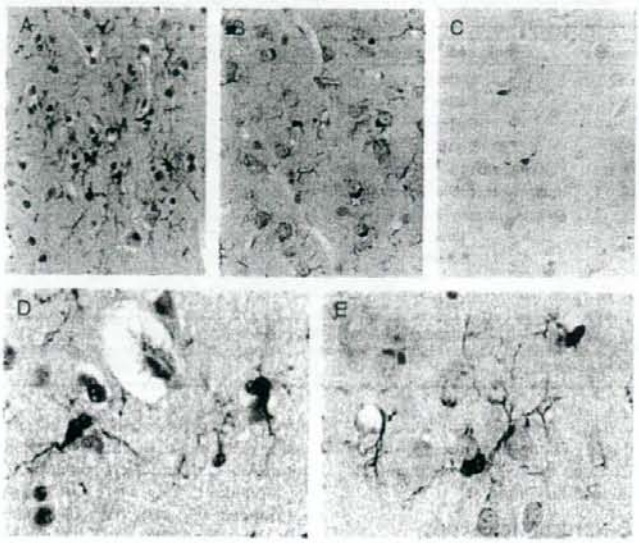

FIGURE 2. Ionized calcium-binding adaptor molecule 1 antibody (Iba1) immunohistochemical staining of activated microglia in the cerebral cortex. Increased Iba1-positive activated microglia are evident in simian immunodeficiency virus (SIV)-infected macaques **(A, B)** compared with the control **(C)**. Some Iba1-positive cells are close to neurons and surround neuronal cell bodies with their extended processes **(D, E)**. **(A, D)** SIVmac239-infected macaque 532; **(B, E)** SIV/human immunodeficiency virus-1-RT-infected macaque 631; **(C)** uninfected control (630). Original magnification: **(A, B)** 400×; **(C)** 100×; **(D, E)** 800×.

behavior. Macaque 730 had the longest clinical course and showed decreased $CD4^+$ cell counts; it was diagnosed as having AIDS at autopsy at 463 weeks. The 3 macaques infected with SHIV-RT also showed decreased $CD4^+$ cell counts and were diagnosed as having AIDS at the time of autopsy. Macaque 631 developed a B-cell lymphoma. All

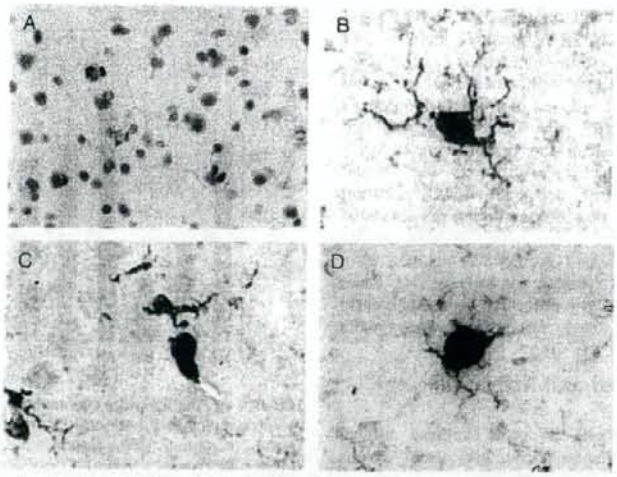

FIGURE 3. Proliferation and activation of microglia in the frontal cortex of animal 631 infected with simian immunodeficiency virus/human immunodeficiency virus-1-RT. Ki-67-positive cells are scattered in the cortical parenchyma **(A)**. Ionized calcium-binding adaptor molecule 1 antibody (binding adaptor molecule 1 antibody (Iba1)-positive microglia with branches **(B)**, amoeboid shape **(C)**, and a large nucleus **(D)** have Ki-67-positive nuclei. **(A)** Anti-Ki-67; **(B–D)** double label of Ki-67 (dark blue) and Iba1 (brown). Original magnification: **(A)** 400×; **(B–D)** 800×.

TABLE 3. Pathologic Findings in Lymph Nodes and Frontal Cortex*

Animal No.	Sex	Viral Inocula	Lymph node Pathology	Decrease of EAAT-2	CD68	GFAP	Ki-67	IL-1β	TNF-α
532	M	SIVmac239	Collapse	1	0–1	2	0–1	0	0
627	M	SIVmac239	Collapse	1	1	1	2	0	1
682	M	SIVmac239	Collapse	0	0–1	1	1	0	0
730	M	SIVmac239	Collapse	3	0–1	3	2	0	0
631	F	SHIV-RT	Follicular atrophy and degeneration	0	0–1	2	2	0	0
677	M	SHIV-RT	Follicular atrophy and degeneration	0	0–1	3	2	0	0
700	M	SHIV-RT	Follicular atrophy and degeneration	2	1	1	3	0	1
630		Control	None	0	1	0	1	0	0
671		Control	None	0	0–1	0	0	0	0
778		Control	None	0	0–1	0	0–1	0	0
780		Control	None	0	0–1	0	0–1	0	0

*, Immunohistochemical staining for each antigen was assessed semiquantitatively by scoring from 0 to 3 in each animal.
EAAT, excitatory amino acid transporter; F, female; GFAP, glial fibrillary acidic protein; IL, interleukin; M, male; SIV, simian immunodeficiency virus; SHIV-RT, SIV/human immunodeficiency virus-1; TNF-α, tumor necrosis factor-α.

SHIV-RT-infected animals had weight loss and were moribund at the time of autopsy. Other than the self-biting behavior in macaque 682, none of the infected animals showed apparent neurologic manifestations.

Histopathology and Electron Microscopy

The animals infected with SIVmac239 and SHIV-RT showed neuropathologic findings as described previously in the cerebral cortex by routine histopathologic examination (27). Briefly, no apparent loss of neurons was detected in the cerebral cortex of any macaques (Fig. 1A). The density of small glial cells seemed to be increased, and they formed apparent perineuronal satellitosis. There were no obvious abnormalities such as pyknosis or chromatolysis evident in the neurons (Fig. 1B). Patchy or diffuse astrocytic gliosis was noted in macaques infected with SIVmac239 (Fig. 1C) and SHIV-RT (Fig. 1D), whereas GFAP-positive staining was limited to the subpial region in the uninfected controls (Fig. 1E). There were no inflammatory infiltrates in the cortex, and there was no evidence of either microglial nodules or MNGCs in the white matter of infected macaques. No abnormalities were observed in the cerebral cortex of 3 uninfected controls. By electron microscopy, the frontal cortex of macaques 532, 627, and 682 showed apparent degenerative changes in the neuropil, including deposition of glycogen-like granules (Fig. 1F), and increased lamellar bodies in the dendrites (Fig. 1G). Foamy changes were detected in the cytoplasm of dendritic trunks (Fig. 1H). There were scattered swollen astrocytic processes because an early reaction of astrocytes and some astrocytic processes were filled with glial fibrils (Figs. 1F, G).

Microglia Are Increased and Activated in the Cerebral Cortex

To characterize the cell involved in these cortical changes, we performed immunohistochemistry using various antibodies, including Iba1, which is restricted to macrophages/microglia (36), and Ki-67, a specific marker of cell proliferation. The cells that increased in number in the cortex were negative for CD3, CD20, or CD68 (data not shown). In contrast, Iba1 immunostaining of SIVmac239- and SHIV-RT-infected macaques demonstrated increased numbers and a wider distribution of Iba1-positive microglia (Figs. 2A, B) compared with uninfected controls (Fig. 2C). Some of the Iba1-positive cells were located close to neurons and surrounded the neuronal cell bodies with their extended processes (Figs. 2D, E). Ki-67-positive cells were increased in the cerebral cortex of SIVmac239 (627 and 730) and all SHIV-RT-infected macaques (Fig. 3A; Table 3). Most of the Ki-67-positive cells were located in the parenchyma, and some positive cells were also closely attached to neuronal cell bodies. Some of the Iba1-positive microglia with ramified processes (Fig. 3B), amoeboid shapes (Fig. 3C), or a large nucleus (Fig. 3D) were also Ki-67 positive by double label immunohistochemistry. Ki-67–positive cells were not

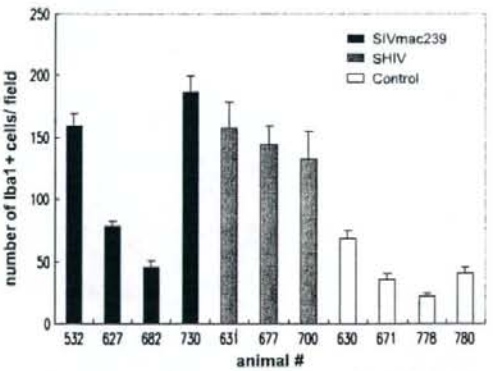

FIGURE 4. Semiquantitative analysis of ionized calcium-binding adaptor molecule 1 antibody (Iba1)-positive cells in the cerebral cortex of simian immunodeficiency virus (SIV)-infected and uninfected control macaques. Ionized calcium-binding adaptor molecule 1 antibody-positive cells were counted in ten 200× magnified light microscopic fields. There were more than twice as many Iba1-positive microglia in the SIV/human immunodeficiency virus-1-RT-infected animals and in 3 of 4 SIVmac239-infected animals as in the controls.

observed among GFAP-positive astrocytes by double label immunohistochemistry with anti-GFAP and anti-Ki-67. Only a few Ki-67-positive cells were found in the cerebral cortex of uninfected controls, and most of them were located near vessels.

In counts of stained cells in 10 microscopic fields at 200× magnification (Fig. 4), the numbers of Iba1-positive cells in all 4 control animals tended to be less than 70 per field. We therefore considered 70 or more cells per field to indicate more Iba1-positive cells. Among the SIVmac239 and SHIV-infected animals, 6 of 7 showed increased Iba1-positive cells. Five showed more than 130 Iba1-positive cells per field, and 1 animal infected with SIVmac239 (627) had 78.2 Iba1-positive cells per field. Another animal infected with SIVmac239 (682) showed no increase in the number of Iba1-positive cells (45.2 per field).

Apoptosis of Astrocytes in SIVmac239- and SHIV-RT-Infected Animals

Our previous study demonstrated astrocytic gliosis, increase in lamellar bodies in the dendrites, and swelling of astrocytic processes in the frontal cortex of macaques infected with SIVmac239 and SHIV-RT (27). To analyze which cell types were predominantly affected, we performed the in situ TUNEL method (Figs. 5A, C, E) and immunohistochemical staining for activated caspase 3 (Figs. 5B, D, F) and ssDNA (Figs. 6E, G) to detect apoptosis. Although the staining results tended to vary in each animal sample, consistent results such as comparable staining patterns in all 3 methods in duplicate can be obtained in samples from SIVmac239-infected (532, 682, 627, and 730), SHIV-RT-infected (700 and 631), and uninfected control (671 and 778) animals.

Terminal deoxynucleotidyl transferase-mediated dUTP-biotin end labeling of fragmented DNA-positive cells were mainly demonstrated in the second layer of the cortex and mostly in glial cells (Figs. 5A, C, E). Some of the positive cells were located close to neurons in SIVmac239-infected (Fig. 5C) and in SHIV-RT-infected animals (Fig. 5E). In activated caspase 3 staining, positive cells showed intracytoplasmic and nuclear labeling (Figs. 6A, C). The numbers of positive cells tended to be high, but most of

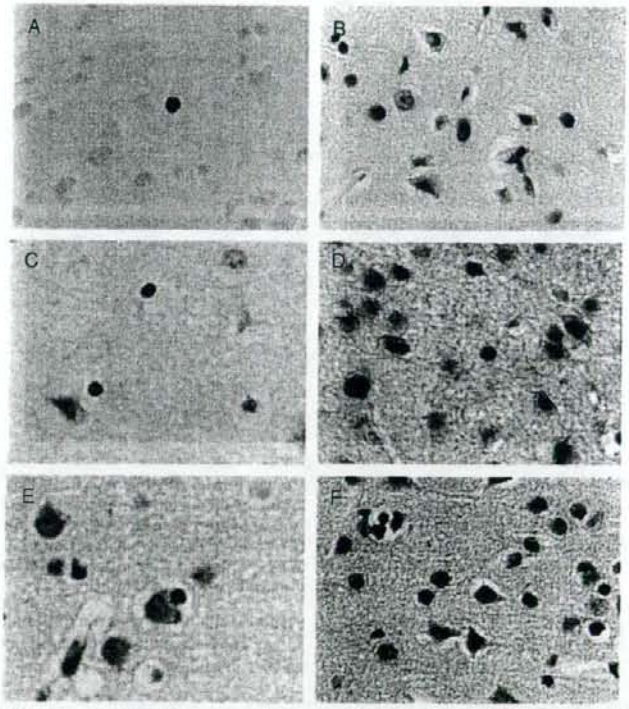

FIGURE 5. ApopTag in situ and anti-activated caspase 3 immunohistochemical staining in the cerebral cortex. Stained glial cells are seen in the simian immunodeficiency virus (SIV)mac239-infected **(A–D)** and SIV/human immunodeficiency virus-1 (SHIV)-RT-infected **(E, F)** macaques. **(A, C, E)**: ApopTag in situ; **(B, D, F)** anti-activated caspase 3. **(A, B)** SIVmac239-infected macaque 532, **(C, D)** SIVmac239-infected macaque 730; **(E, F)** SHIV-RT-infected macaque 700. Original magnification: **(A–F)** 400×.

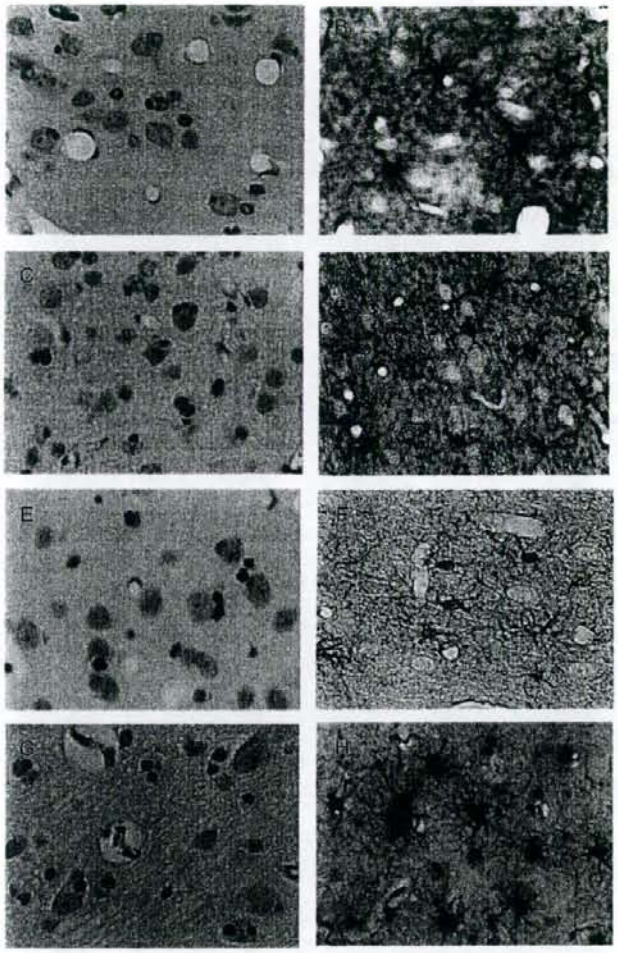

FIGURE 6. Double label immunohistochemistry with anti-glial fibrillary acidic protein (GFAP) and anti-activated caspase 3 or single-stranded DNA antibody (ssDNA) in the cerebral cortex of the simian immunodeficiency virus (SIV)mac239- and SIV/human immunodeficiency virus-1 (SHIV)-RT-infected animals. Most of the doubly positive cells are astrocytes with small round nuclei. **(A, C)** Anti-activated caspase 3; **(E, G)** anti-ssDNA; **(B)** double label anti-activated caspase 3 (brown) and GFAP (dark blue); **(D)** double label anti-activated caspase 3 (red) and GFAP (dark blue); **(F)** double label ssDNA (red) and GFAP (brown); **(H)** double label ssDNA (dark blue) and GFAP (brown); **(A, B, E, F)** from SIVmac239-infected macaque 682; **(C, D)** from SHIV-RT-infected macaque 631; **(G, H)**from SHIV-RT-infected macaque 700. Original magnification: **(A–H)** 400×.

the positive cells seemed to be glia (Figs. 5B, D, F). The ssDNA-positive cells showed nuclear labeling and also seemed to be glia (Figs. 6E, G). Based on double label immunohistochemistry (Figs. 6B, D, F, H), more than half of the activated caspase 3 and ssDNA-positive cells were also positive for GFAP. Some of the activated caspase 3 and ssDNA-positive cells seemed to be microglia according to the shape of their nuclei. No apparent neuronal staining with these markers of apoptosis was observed. Only very few positive cells were detected in the uninfected controls by the in situ TUNEL method and based on activated caspase 3 and ssDNA immunostaining.

EAAT-2 Expression

The expression of Na^+-dependent glutamate transporters (EAAT-1 and EAAT-2) primarily on astrocytes is thought to keep the extracellular glutamate concentration low in the brain and prevent excitotoxicity to neurons. In all

animals studied, EAAT-2 expression was predominantly in the neuropil of the cerebral cortex. A diffuse decrease in EAAT-2 expression and scattered astrocyte staining in the neuropil were observed in SIVmac239-infected animal 730 (Fig. 7A) and SHIV-RT-infected animal 700 in contrast to the diffuse staining in the control animals (Fig. 7B). The 2 infected animals had very long durations of SIV infection: 463 and 263 weeks, respectively. A patchy decrease in EAAT-2 expression was observed in SIVmac239-infected animals 627 (Fig. 7C) and 532. In addition, we observed a strong expression of EAAT-2 by microglial cells, some of which came in close contact with neurons and blood vessels in SIV-infected animals (Fig. 7D), as demonstrated by double label immunofluorescence with anti-Iba1 and anti-EAAT-2 (Figs. 7E–G). The decrease in EAAT-2 in the neuropil seemed to be mild when the activated microglia expressed EAAT-2 (Fig. 7D).

Diffusely Activated Microglia Do Not Express TNF or IL-1β

To clarify the role of microglial activation in the frontal cortex, we examined expression of the potentially harmful proinflammatory cytokines. Cells positive for IL-1β and TNF were detected in the marginal zone of follicles of the positive control tonsil, but IL-1β and TNF were not detected in the cortex where the microglia were diffusely activated. However, TNF was detected in a few perivascular cells of SIVmac239-infected (627) and SHIV-RT-infected (700) macaques (Table 3).

SIV Infection Is Undetectable in the Frontal Cortex of SIV-Infected Animals

We performed immunohistochemistry for SIVenvgp160/gp32 to detect virus-infected cells in the frontal cortex in which astrocytic gliosis and microglial activation were observed. No SIVenvgp160/gp32-positive cells could be detected in the cerebral cortex of any SIV-infected animals. Only a few mononuclear cells were positive in the meninges of the macaque 682 infected with SIVmac239. To confirm the absence of SIV-infected cells in these cortical lesions, nested PCR was carried out on genomic DNA extracted from 3 different parts of paraffin-embedded frontal lobe sections, that is, the frontal cortex parenchyma, perivascular areas of the frontal cortex, and the white matter, using AS LMD. Our PCR system detected a single copy of *SIV gag/SIV env* genes in 100 cells by a sensitivity assay using SIV plasmid DNA diluted with DNA from paraffin-embedded lymph node sections of an uninfected macaque. Although strong bands can be easily detected by PCR of SIV DNA in infected lymph nodes, no positive bands were obtained from the

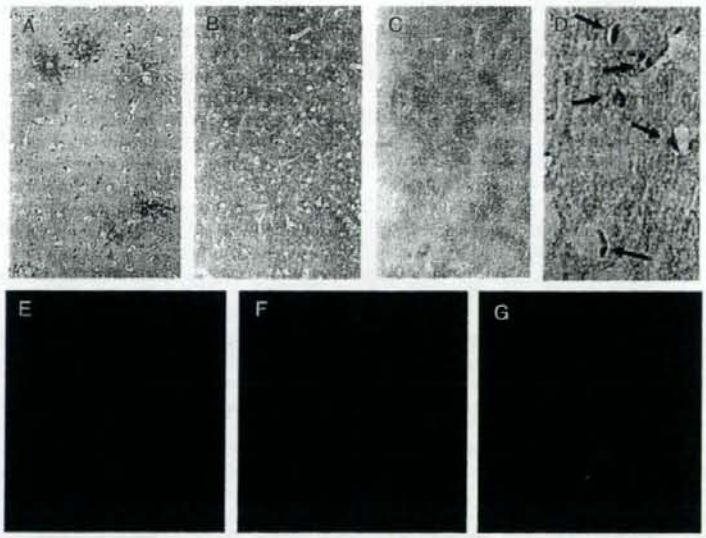

FIGURE 7. Decreased excitatory amino acid transporter (EAAT) 2 expression and EAAT-2 expression by microglia in the cortex of simian immunodeficiency virus (SIV)mac239-infected animals. A diffuse decrease in EAAT-2 (**A**; 730) and patchy decrease in EAAT-2 (**C**; 627) contrast with diffuse staining in the uninfected control animal (**B**; 671). In animal 627, strong EAAT-2 expression was noted on perineuronal and perivascular cells (arrows), and the decrease in the expression of EAAT-2 in the neuropil seemed mild (**D**; 627). Activated microglia expression of EAAT-2 is demonstrated by double label immunofluorescence with anti-ionized calcium-binding adaptor molecule 1 antibody (Iba1) and anti-EAAT-2 (**E–G**; 627). **(A–E)** Excitatory amino acid transporter 2; **(F)** Iba1; **(G)** merged. Original magnification: **(A–C)** 100×; **(D–G)** 400×.

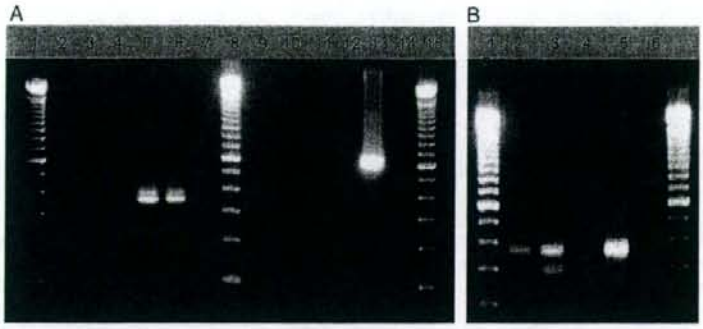

FIGURE 8. Detection of simian immunodeficiency virus (SIV) gag and env DNA in SIVmac239-infected macaque 532 in LCM microdissected tissues by PCR. The blots illustrate SIV gag (Lane A-2 to A-7) and env (Lanes A-9 to A-14), and β-globin (Lanes B-2 to B-6) amplified DNA from parenchymal (Lanes A-2 and A-9; B-2) and perivascular areas (Lanes A-4 and A-11; B-4) of the frontal cortex, and white matter (Lanes A-3 and A-10; B-3) of macaque 532. Lanes A-5, A-6, A-12, and A-13 are positive controls with 1 copy of plasmid DNA (Lanes A-5 and A-12) and 4 copies of plasmid DNA (Lanes A-6 and A-13). Lane B-5 is a positive DNA control from lymph node sections of 682. Lanes A-7, A-14, and B-6 indicate distilled water used as a polymerase chain reaction control without template DNA. Lanes A-1, A-8, A-15, B-1, and B-7 are molecular weight standards.

DNA samples of any of the 3 regions of the frontal lobe of the SIVmac239-infected animal (Fig. 8).

DISCUSSION

In this study, we examined the cortical pathology seen in animals infected with T-cell-tropic SIV, especially focusing on the change in the astrocytes and microglia. We observed abnormalities of astrocytes, including apoptosis and a decreased expression of EAAT-2 in the neuropil. We used 3 different methods, TUNEL and immunohistochemistry for activated caspase 3 and ssDNA to analyze apoptosis, and found that most positive cells were astrocytes by all 3 methods. Although the numbers of caspase 3- and ssDNA-positive cells seemed higher than expected, the concordance of the results of all 3 methods and double immunohistochemistry suggested a predominant involvement of astrocytes in the frontal cortex of SIV-infected animals. The apoptosis of astrocytes might be observed under physiologic conditions whereby the brain removes any excessive astrocytes that have proliferated after certain types of brain injury (38). Proliferation of astrocytes was not a plausible explanation in this study because Ki-67-positive astrocytes could not be detected by double label immunohistochemistry (data not shown). Another astrocytic change observed was a remarkable decrease in the expression of EAAT-2 in the neuropil in animals with a prolonged duration of SIV infection because a major cellular component of the brain astrocyte have important effects on neuronal biology by buffering the extracellular milieu, providing cytoskeletal support, and protecting neurons during CNS injury. The neuroprotective role of astrocytes has been described in connection with the expression of glutamate transporters (EAAT-1 and EAAT-2). The astrocytes maintain a low extracellular glutamate concentration in the brain. Glutamate, the major neurotransmitter in the CNS, induces excitotoxic neuronal cell death when its extracellular concentration increases, and it is also believed to be an important factor in the pathogenesis of many CNS disorders, including amyotrophic lateral sclerosis, Huntington disease, Alzheimer disease, and multiple sclerosis (39–43). The present findings suggest that astrocytes in the cerebral cortex are also primarily involved in the pathogenesis of AIDS encephalopathy.

We found diffuse activation of microglia in the cortex of infected animals and some of the activated microglia expressed EAAT-2; expression of TNF and IL-1β was not detected by immunohistochemistry. In general, microglia are distributed ubiquitously throughout the CNS and become activated in response to harmful stimuli (44). Activated microglia release proinflammatory cytokines such as IL-1β and TNF and thus mediate a neurotoxic function (29, 30). On the other hand, activated microglia may also secrete neurotrophic factors and provide neuroprotective functions (45). The expression of EAAT-2 by microglia has been reported in both AIDS brains (33, 34) and in SIVmac251-infected macaques (46). We confirmed the EAAT-2 expression by activated microglia in our model. The decrease in the expression of EAAT-2 in the neuropil seemed to be mild where activated microglia expressed EAAT-2. These data suggest that microglia might, like astrocytes, clear extracellular glutamate, thereby playing a neuroprotective role in the cortical degeneration seen in AIDS brains.

The involvement of the cerebral cortex in ADC is one of the major pathologic changes, and this phenomenon is called DPD (11). Neuron loss and apoptosis are believed to be the primary lesion in DPD. In our model, however, we observed only mild neuronal damage, that is, ultrastructural changes of dendrites. Because, with only 1 exception, our animals did not show any neurologic signs, we suspect that neuroprotection by activated microglia was efficient, and that this may also explain the absence of neuronal loss. Another possible explanation might be the difference in the stage of DPD. In human ADC, an autopsy is usually performed at the advanced stages such as in patients demonstrating a